

# We are IntechOpen, the world's leading publisher of Open Access books Built by scientists, for scientists

6,900

Open access books available

186,000

International authors and editors

200M

Downloads

Our authors are among the

154

Countries delivered to

TOP 1%

most cited scientists

12.2%

Contributors from top 500 universities



WEB OF SCIENCE™

Selection of our books indexed in the Book Citation Index  
in Web of Science™ Core Collection (BKCI)

Interested in publishing with us?  
Contact [book.department@intechopen.com](mailto:book.department@intechopen.com)

Numbers displayed above are based on latest data collected.  
For more information visit [www.intechopen.com](http://www.intechopen.com)



# Superconducting Devices in Wind Farm

Xiaohang Li

*Innova Superconductor Technology Co. Ltd. Beijing*

*China*

## 1. Introduction

Wind power is very promising in the near future and drawing more and more attentions from the governments and enterprises world wide. The global wind power industry expanded rapidly in the recent several years. In 2009, the world's total generation capacity of wind power was 157.9 million kW, of which ~ 31% was newly installed within the year. From industrial reports, the installed wind power capacity will increase by more than 30% per year in the following decade, especially in China, where GDP and power consumption are boosting quickly. It is estimated that in China, the installed wind power capacity will exceed 150 million kW and supply ~ 15% of the country's needs by the year of 2020.

In a common view, wind energy is clean, renewable and abundant. The estimated global resource of wind power is up to  $2.74 \times 10^{12}$  kW, while the exploitable capacity is  $\sim 2 \times 10^{10}$  kW. Further more, wind power is free of environmental impacts compared to traditional power resources, such as the hydro, thermal and nuclear power. However, energy density of wind power is low, and the wind energy resources are distributed, i.e., the majority of them is located in the rural areas, the coasts and the offshore sea shelves. At the background of global energy shortage, governments and enterprises are pushing forward the construction of new and large wind farms in these outfields. In the past several years, following the quick developments of wind power plants in the plains and highlands, the United States, Japan and Europe began to install offshore wind power turbines. For example, in April 2010, the first offshore wind plant in Germany was installed in the North Sea. This plant consisted of twelve 5 MW turbines, with annual power generation capacity of 220 million kWh.

The brilliant future of wind power emphasizes the motivation on the technical upgrades in the wind farms, including the introduction of various high temperature superconducting (HTS) devices. In the past decade, many research and test operation efforts were paid on the new and high efficiency power applications, such as "direct- driven" permanent magnet (PM) generators and HTS generators; magnet, flying-wheel and battery energy storage systems; fault current limiters; solid state transformers and electronic voltage regulators. These devices are designed to solve the problems occurring in the quick boosting up of the wind farms and the strict requirements on connecting them to the main frame of the power grids. Generally, these problems can be described as the optimization of the generator capacity, the size and weight of the wind turbine system, the stability of the output, as well as the tolerance of the system against fluctuations from the driving force, aka the wind, and the load. One of the key approaches to achieve the optimization is the superconducting

technology. Following this approach, a series of HTS devices were proposed, including HTS generators, superconducting energy storage systems (SMES), superconducting fault current limiters (SFCL), HTS transformers and HTS power transmission cables. This chapter is a basic introduction to the design and tentative application ideas of these devices. Following this part, there are 5 parts on the basic knowledge of superconductivity and HTS materials, HTS generators, SMES, SFCL and other HTS devices such as HTS cables. At the end of this chapter is a short conclusion outlining the future superconducting wind farms.

## 2. Basic knowledge of high temperature superconductor

In 1911, superconductivity as a physical phenomenon was discovered by Kamerlingh Onnes (H. Kamerlingh Onnes, 1911) during the low temperature conductivity measurement of Hg. In his experiment shown in Figure 1, when the temperature dropped to 4.2 K, the resistance of Hg dropped to below the limit of the measurement device, and virtually taken as zero. From then on, superconducting technology became more and more attracting in various areas, including energy, information, transport, medical, scientific instruments, defense, etc. Two key physical properties are identified in superconductor, one is zero resistance and the other is complete diamagnetic phenomenon. In electrical power application, zero resistance is often utilized as it implies high current capacity and extremely low Ohmic loss. However, diamagnetic and superconducting-normal state transition properties are also of important practical value.

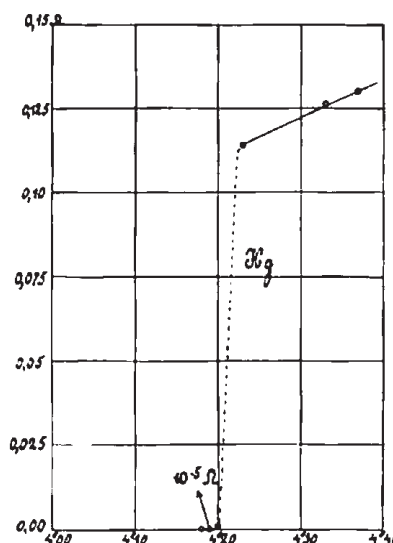


Fig. 1. The zero resistance transition of Hg measured in 1911 by Kamerlingh Onnes.

Utilizing the high current density and consequently high magnetic field density generated by the current, superconducting coils, cables, generators, motors, transformers and magnetic energy storage systems are invented and developed. Besides, based on the state transition, superconducting device can be with no resistance while carrying a current below designed value and with pronounced resistance when the current exceeds that, which makes it an excellent candidate to fault current limiter. In modern wind farm designed to supply large amount of electrical power to the main frame of the grid, superconducting devices are now widely considered. Basic knowledge of the key physical properties in superconductor will be introduced in the following several pages.

## 2.1 Critical parameters in superconductor

In a given superconductor, zero resistance can only occur below certain temperature and external magnetic field, while carrying a transport DC current below certain density at the same time. The three limitations are thus called the “critical” temperature, field and current density of the superconductor, denoted by  $T_c$ ,  $H_c$  and  $j_c$ , respectively. As shown in Figure 2, the critical limitations are correlated with each other. When two of the external parameters are zero, the limitation on the third depends only on the intrinsic properties of the material. In the other cases, superconductivity only occurs at the environmental conditions below the surface formed by  $T_c$ ,  $H_c$  and  $j_c$  as functions of the temperature, field and current density. In another word, the superconductor is in superconducting state only when the environmental parameters are below this surface and in the normal state otherwise. In superconductors reported so far, the highest  $T_c$  is about 160 K; the maximum theoretical  $H_c$  is up to 100 T, while the highest practical  $H_c$  is over 25 T; and the highest  $j_c$  is up to  $10^7 \text{ A/cm}^2$  in epitaxial thin HTS films.

As described above, only when the ambient temperature drops below certain value, aka  $T_c$ , can a superconductor begin to show superconductivity. In a practical superconductor, the normal to superconducting state transition occurs in a temperature range around  $T_c$ . This range is then called the transition width. In HTS materials, the transition width is usually about 0.5 - 1 K, depends mainly on material homogeneity. The so called “high temperature” for superconductor implies  $T_c$  is usually higher than the liquid nitrogen temperature (77 K). Similar to  $T_c$ , at certain external magnetic field  $H_c$ , superconductivity is suppressed too.  $H_c$  is temperature dependent and generally decreasing with temperature increasing. The field and superconductivity interaction is material dependent. Some materials allow no magnetic flux penetrates into, so they have only one  $H_c$  and are called “Type I” superconductors. The others allow partially flux penetration at fields above  $H_{c1}$  while zero resistance disappear only at fields higher than  $H_{c2}$  and then called “Type II” superconductors. Figure 3 shows the magnetization behavior of two types of superconductors. Practically used superconductors are usually Type II as Type I superconductors can only carry transport current in a very thin layer close to the surface, which makes it almost impossible to be used in the high current and field devices. In HTS materials, there is a special magnetic phenomenon at field called irreversible field  $H_{irr}$ , above which the magnetization is reversible because the flux is able to “creep” freely in the superconductor. At fields beyond  $H_{irr}$ , although HTS material is still with zero resistance, the free flux creeping makes it hardly to carry any transport currents as the field generated by the transport current can drive the flux out and consequently extinguish the current.

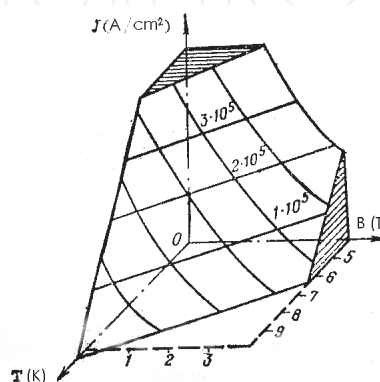


Fig. 2. Scheme of the correlations among the three critical limitations in superconductor.

In superconductor, at certain temperature and external field, resistance will generally recur when the transport current density is above certain value,  $j_c$ . In applications, critical current of superconductor, denoted by  $I_c$  is commonly used instead of  $j_c$ .  $I_c = j_c S$ , where  $S$  is the current-carrying cross-section. Since zero resistance is difficult to detect using conventional measurement devices, in engineering,  $I_c$  is often defined as the transport current carried by the sample when the electrical field across its length reaches  $1 \mu\text{V}/\text{cm}$ .

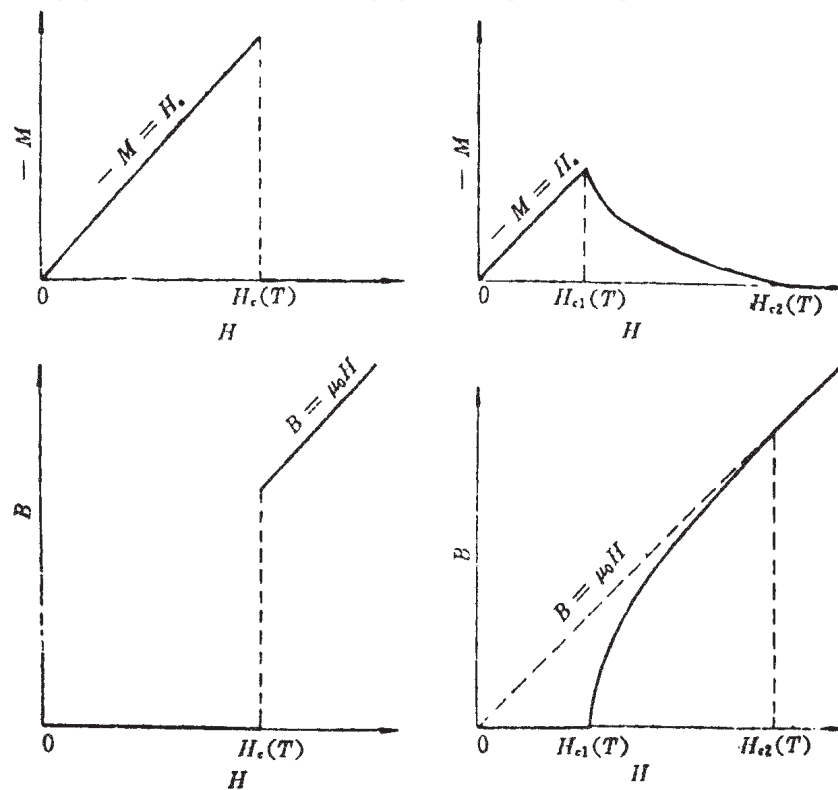


Fig. 3. Scheme of magnetization in Type I (left) and Type II (right) superconductors.

Due to zero resistance, superconducting materials can be jointed into a closed circuit, and a continuous current excited in this circuit can last for several years without significant decay. Measurement via such continuous current approach shows the upper limit of the resistivity in a typical superconductor is less than  $10^{-26} \Omega\text{cm}$ . It implies a potential application value of extremely low energy losses in various areas correlated with electricity and magnetic field. However, among more than 4000 so far discovered superconductors, only  $\sim 10$  of them are widely utilized. The three "critical" parameters, aka  $T_c$ ,  $H_c$  and  $j_c$  are very important to the practical value of a superconductor. For example, discovery of HTS materials was the most exciting event in the late 1980s because it opened a new front of applied superconductivity characterized by low energy cost and high efficiency, especially in the renewable electrical power area by allowing the operation of superconducting devices in the comparatively cheap and convenient environment of liquid nitrogen temperature.

## 2.2 The E-I correlation

In a superconducting device design, the most important parameter to decide is the working current. It depends on both  $I_c$  and the voltage - current correlations in the material. Apply a transport DC current  $I$  to a sample and record the voltage  $U$  across it, normalize  $U$  to the

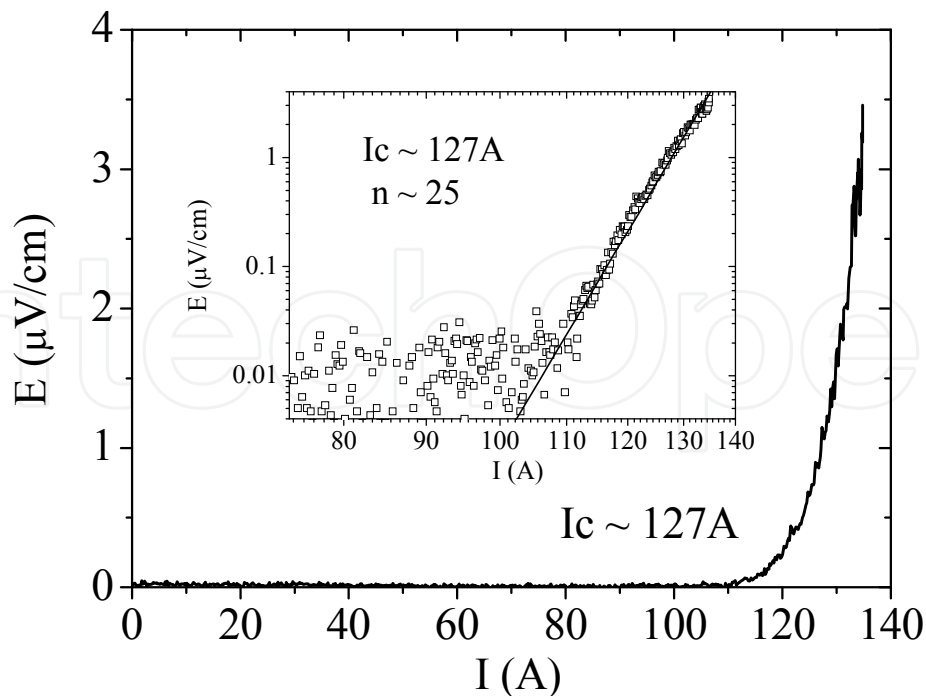


Fig. 4. The electric field - current (E-I) correlations measured in HTS wire at 77 K, self field. The inset plots the same curve in exponential coordinates to show the estimation of  $n$  value.

sample length  $l$  as the electric field  $E = U/l$ , the voltage - current correlations in the sample can be illustrated as Figure 4. With  $I$  increasing, initially the sample shows zero resistance,  $E$  is zero. When  $I$  rises to near  $I_c$ ,  $E$  starts to rise rapidly with  $I$ . The E-I curve in this stage is commonly nonlinear. Finally, when  $I$  is much larger than  $I_c$ , the sample is fully transferred into the normal state, the E-I curve becomes linear and satisfying the Ohm's law,  $E = IR_n/l$ . Here  $R_n$  is the normal state resistance of the sample. A so called "power law" was proposed to describe the E-I correlations at transport current  $I$  around  $I_c$ :

$$E = E_0(I/I_c)^n \quad (1)$$

In practical measurements,  $E_0$  and  $n$  can be regarded as fitting parameters. According to the engineering criterion of  $I_c$ ,  $E_0 = 1 \mu\text{V}/\text{cm}$ , while  $n$  is sample dependent. In a completely homogeneous sample,  $n$  represents the intrinsic properties of the superconductor. However, due to microstructure distributions and impurities, transition from superconducting to the normal state in a practical sample is usually inhomogeneous, the E - I correlation curve is then broadened in transition width and  $n$  is also smaller than the theoretical. In practical usages, especially where superconducting wires are concerning, it is generally believed that the greater the  $n$  value, the better uniformity of the material, aka the material will transfer into and out of the superconducting state more simultaneously at given environment. Thus, in magnets and superconducting power devices, which commonly use a pronounced length of superconducting wires,  $n$  value is important. The  $n$  value in commercial low temperature superconducting materials such as NbTi multi-filament wire is more than 40, much larger than that in HTS wires. For example, in Bi2223/Ag wire,  $n$  is generally less than 30, while in YBCO coated conductor,  $n$  can be comparatively larger. It is believed that the ceramic nature of HTS materials, i.e., the grainular structure, disorder region and/or the angles between the grain orientations are reasons for the comparatively bad homogeneity and small  $n$  value.

### 2.3 The AC losses

Zero resistance only occurs in the superconductor carrying DC current less than  $I_c(B,T)$  and at stable or zero background electromagnetic fields. In AC cases or at alternating fields, due to forced movements of the magnetic flux, there will be energy losses in the superconductor, which usually called AC losses. In bulk or single filament materials, AC losses are mainly the hysteresis loss. The definition of hysteresis loss is in analogy to that in FM materials, when a superconductor is applied to alternating magnetic fields either from AC transport current or the environment, magnetic flux lines will enter and exit, and the work done to overcome the flux pinning forces is the hysteresis loss. Thus, hysteresis loss is proportional to frequency. In multi-filament superconducting wires, in addition to hysteresis loss, there are coupling loss and eddy current loss. The coupling loss comes from the lateral flow of the current in the sheath material between the filaments, and is proportional to the square of the frequency. The eddy current loss comes from the Ohmic loss of the eddy current induced by alternating magnetic field in the normal metal sheath around the superconducting core, and is also proportional to the square of the frequency. For electrical engineering, where the frequency is 50 or 60 Hz, the hysteresis loss is dominant in common practical HTS materials. Nevertheless, AC losses in superconductor are much smaller than the Ohmic loss in normal metal conductor while transmitting the same current. Thus, using HTS materials are energy saving in AC devices if AC losses and the cooling conditions are carefully considered. Methods to estimate AC losses were proposed by researchers based on critical models of the superconductor and proofed qualitatively in applications (W. T. Norris, 1969, W. J. Carr, Jr. 1983). To reduce the AC losses, thin filament wires and special wire design such as using high resistivity material as barrier layers of lateral and eddy currents are developed. For precise researches considering flux creeping and microstructure distributions, especially in practical HTS wires with obvious inhomogeneity, finite element methods are suggested.

### 2.4 Properties of HTS materials

The emergence of high-temperature oxide superconductors broke the temperature barrier of applied superconductivity by switching the working temperature from liquid helium (4.2 K) to liquid nitrogen (77 K). Hence, HTS devices can be small, light and efficient, with high working current density and, as the most important advantage, cheap cooling cost. By now there are several series of HTS materials discovered: La-Ba-Cu-O, ( $T_c = 35$  K), Y-Ba-Cu-O ( $T_c = 92$  K), Bi-Sr-Ca-Cu-O ( $T_c = 110$  K), the Tl series ( $T_c = 125$  K) and the Hg series ( $T_c = 135$  K). Among them Y-Ba-Cu-O and Bi-Sr-Ca-Cu-O composites are the most promising in practical applications. The crystal structures of  $\text{Bi}_2\text{Sr}_2\text{CaCu}_2\text{O}_8$  (Bi2212),  $\text{Bi}_2\text{Sr}_2\text{Ca}_2\text{Cu}_3\text{O}_{10}$  (Bi2223) and  $\text{YBa}_2\text{Cu}_3\text{O}_7$  (Y123 or YBCO) are shown in Figure 5.

As shown in Figure 5, HTS materials are copper oxide with layered structures of complex perovskite. They are obviously anisotropic, with very different physical properties along the perpendicular and parallel directions of the copper-oxygen layer. Bulks and wires made of HTS materials have been developed in the decades after their discovery. Among them, the most promising ones are the Bi2223 and YBCO wires. Bi2223 has a derivative of perovskite structure with pseudo-tetragonal symmetry (space group  $I4/mmm$ ) as shown in Figure 5b. Its coherence length is very short, at the direction along the copper-oxygen surface is  $1 \sim 2$  nm, perpendicular to the surface is much less than 1 nm. Thus, in strips of Bi2223, current must flow through the grain boundaries, and only well aligned grains can transport significant current. The layered structure of Bi2223 makes it possible to obtain good textured

strips using mechanical deformation and heat treatment, a powder in the tube (PIT) method was then developed to manufacture Bi2223 wires. Now, commercial Bi2223 wires are available in the length of several hundred kilometers per year, with a price of about \$ 90 /kA.m. Such wires with cross-section of  $\sim 1 \text{ mm}^2$  can transport  $\sim 150 \text{ A}$  DC current when cooled in liquid nitrogen immersion. It opens many possibilities in practical power devices such as transmission cables. However, although the theoretical  $H_{c2}$  of Bi2223 is up to 25 T, much larger than that of NbTi and Nb<sub>3</sub>Sn, at 77 K,  $j_c$  in Bi2223 wire drops quickly as the magnetic field rising, makes a serious drawback to the applications in electromagnetic devices such as SMES, motors, generators and transformers. Besides, the mechanical strength and AC properties in Bi2223 wire are also to be significantly improved for practical usages. On the other hand, YBCO wires were developing very fast in the past decade and now often regarded as the succession of Bi2223. In industrial reports, YBCO wires are usually called as the "second generation" HTS wires. The structure of YBCO is also layered perovskite, as shown in Figure 5c. It has an orthorhombic symmetry (space group Pmmm).

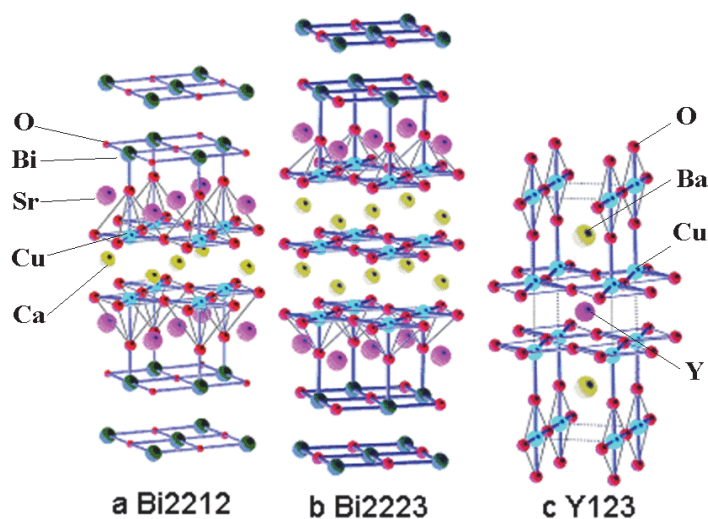


Fig. 5. Crystal structures of HTS materials: (a)  $\text{Bi}_2\text{Sr}_2\text{CaCu}_2\text{O}_8$  (Bi2212), (b)  $\text{Bi}_2\text{Sr}_2\text{Ca}_2\text{Cu}_3\text{O}_{10}$  (Bi2223) and (c)  $\text{YBa}_2\text{Cu}_3\text{O}_7$  (Y123 or YBCO).

The  $c$  lattice constant is about 3 times of that of  $a$  and  $b$ , so it also shows significant anisotropy. Unlike Bi2223, it is difficult to prepare good textured YBCO wire using PIT method. Instead, YBCO coated conductor wires deposited on biaxial textured metal tape substrates was invented and commercialized. A schematic structure of this wire is shown in Figure 6.  $H_{c2}$  in YBCO at 77 K is much higher than that in Bi2223, so the  $j_c$  - magnetic field correlations in YBCO wires is also much better. It is believed that YBCO wires will take the part of Bi2223 wires in most power applications, and further push forward the wide applications of HTS materials in the magnetic devices. The drawbacks of YBCO wires now are the difficulties of producing large amount of wire in comparatively cheap prices.

### 3. HTS generator

Decades ago, capacity of wind turbine was in the scale of kW and wind farms were mostly isolated from the power grid, and supplying power to the rural villages. At present, capacity of wind farms are becoming comparable to the hydro and thermal plants, and wind power

is going to play an important role as a major energy resource connected to the main frame of electrical services. The rapid scaling up of the wind farm demands not only large number of turbines, but also high energy density and efficiency in them. It is now widely accepted that HTS devices are promising in wind farms because the energy density in HTS devices can be 10 times larger than that in the common ones, with less than 1/3 the energy costs at the same time. Among the proposing devices, HTS generators are the most attracting. Several reports concerning 8-10 MW HTS generators developing in the States, Europe, Japan and China have been published.

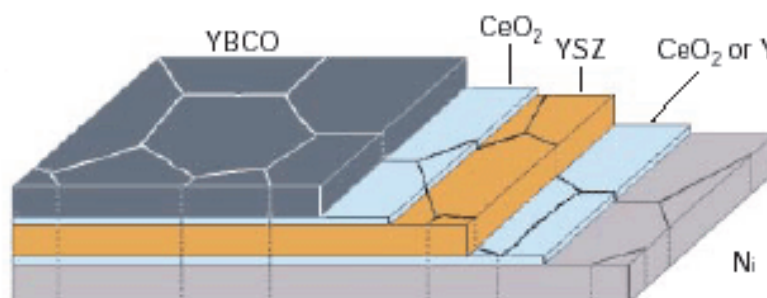


Fig. 6. A schematic structure of the YBCO coated conductor wire.

### 3.1 Conceptual design

As the capacity of the wind farm grows rapidly, the wind turbine also scales up quickly. At present, 2 - 3 MW wind turbines are the hot sale in the wind power industry, while turbines with the capacity of more than 5 MW are also successfully commercialized world wide. Two types of generators are currently installed in wind farms, one is high speed "doubly-fed" asynchronous and the other is low speed "direct-driven" synchronous. The former is light and compact, structured in much analogy to the generators using in the thermal plants, with 2 or 4 poles and rotates at a speed of 1500 - 3000 rpm. A complex gear system must be connected between the wheel and the generator to multiply the rotation speed as the blade velocity of the wind wheels cannot be very high. On the contrary, the latter rotates at a speed close to the wheel, which is commonly less than 150 rpm, and the gear system is simple, if cannot be omitted. The capacity of the "doubly-fed" generator is usually less than 3 MW, while the "direct-driven" PM generators are advantageous in size and weight in the capacity range of 2 - 5 MW. At 5 - 6 MW, the weight of both of the "direct-driven" PM generators and the gear box of the "doubly-fed" generators will be at the altitude of 100 tons. It makes a serious drawback to the economic benefit of the wind farm. Using HTS materials instead of permanent magnets is a proposed approach to overcome the size and weight problems in the large capacity "direct-driven" generators, because the electromagnetic field density in the HTS magnets are much larger than that in the permanent magnets.

Fig. 7 is a schematic diagram of a "direct-driven" HTS generator system illustrating the design concept. The system consists of a wind wheel, a simple/optional gear system, a HTS generator, a stand alone excitation power supply, a cooling system, a converter and a transformer connecting to the power grid. In this diagram, the wheel and the gear system are similar to those in the 3 - 5 MW "direct-driven" PM generators, but the capacity is larger and the rotary speed is also slower. For example, in 10 MW wind turbine systems, the rotary speed of the wheel is usually 8 -12 rpm, while the speeding up ratio of the gear box, if

necessary, can be 5 - 10 for the size and weight optimization in both of the generator and the gear system. The HTS generator used here is hybrid structured as widely suggested, i.e., its rotor is made of HTS materials and the stator is conventional. Fig. 8 shows a schematic diagram of the hybrid structured HTS generator. It consists of the HTS rotor, supported by torsion transmitting tubes and sealed in a cryostat (often called Dewar in scientific reports), and a conventional stator. For the convenience of connecting to the grid, the output voltage of the system  $V$  is often selected as the common values used in the substations, for example, 10.5 kV and 35 kV in China. Similarly, the output of the system is usually in 3 phases, the same as that in power grid. Thus, for designed capacity  $P$ , the output current  $I = 0.577P/V$ .

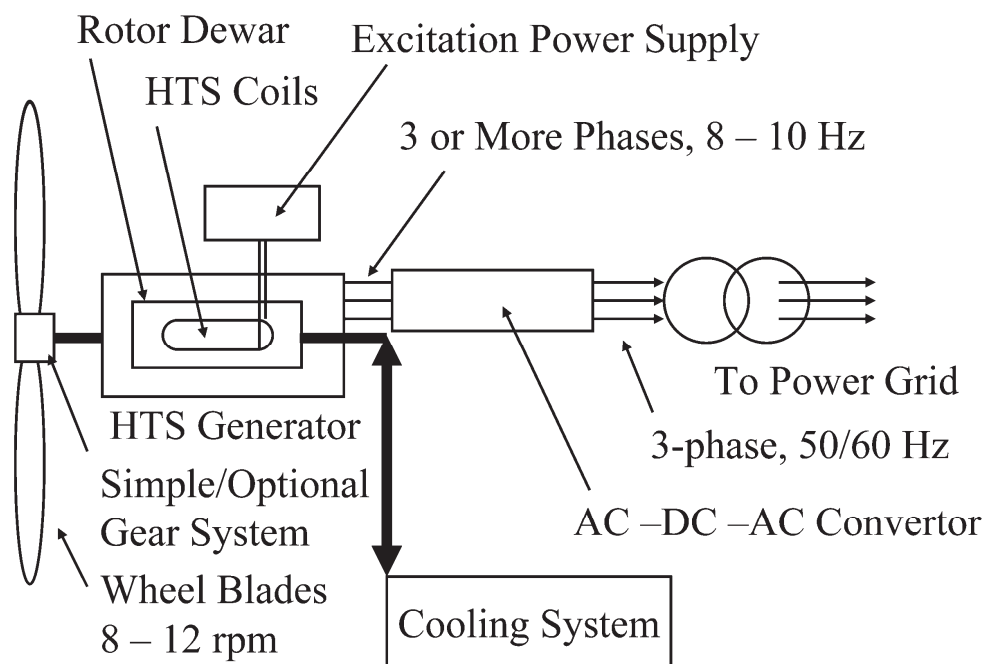


Fig. 7. The schematic diagram of a HTS generator system.

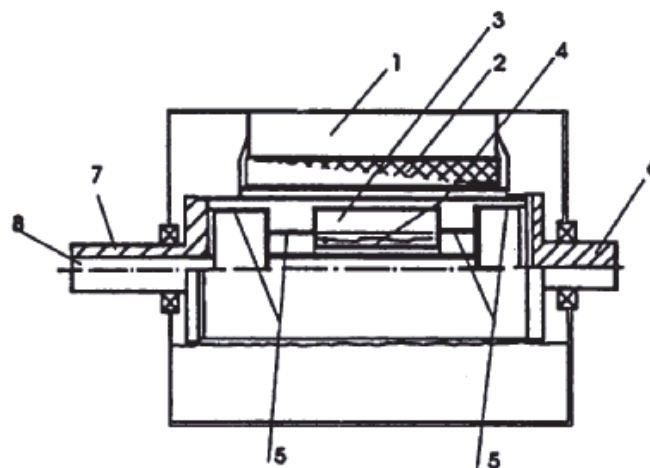


Fig. 8. The schematic diagram of the hybrid structured HTS generator. Labels in the figure: 1, Stator iron core; 2, Stator coil; 3, HTS rotor coil; 4, Rotor Dewar; 5, Torsion transmitting tube; 6, Driving shaft; 7, Supporting tube; 8, Axial tube for cooling and current transition.

However, adjusted by converter and transformer, the number of phases in the generator, as well as the generator output voltage  $V_g$  and the stator phase current  $I_g$  are not necessarily the same as those of the system, and can be optimized in generator electromagnetic design. It is note worthy that adopting an AC - DC - AC converter between the generator and the transformer, the output frequency of the generator  $f_g$  can also be adjusted. It is usually very low although the system output frequency  $f$  is commonly 50 or 60 Hz according to the grid standards. This is advantageous because the number of magnetic poles in the rotor  $2p$ , which can be calculated by  $n = 60f_g/p$ , decides the generator size and weight provided the materials are the same. Reducing  $p$  is particularly beneficial in the "direct-driven" HTS generators as the minimum bending diameters of commercial HTS wires are usually about 40 - 70 mm, which makes it difficult to wind magnetization coils smaller than NdFeB bulks, and a rotor with many pairs of HTS coils would be large. In common,  $f_g$  in a HTS generator of several MW capacity can be 8 - 10 Hz to meet the speed requirement of the turbine, the optimized coil size and weight, and electromagnetic design convenience at the same time. Since DC resistance in HTS material is extremely small and only DC excitation current is used for synchronous generator, the excitation power requirement of HTS generator is very low. However, the field density in HTS coil is much larger than that in conventional ones, the excitation current must be very stable, a stand alone power supply is then suggested for exciting the HTS coils. Its input power can be in the altitude of 10 kW, while the output current is 100 - 200 A, with very low fluctuations. Superconducting magnet power supply made by the Bruker Corp. can be a good candidate for this. In emergency, this device can even be activated by a set of batteries.

Besides the power supply, a cooling system is also necessary to the HTS generator. Depends on the capacity and the rotor design, around 500 - 1000 W cooling power is needed. This can be supplied by Stirling or G-M coolers, which give 200 - 500 W cooling power at  $\sim 77$  K with 5 - 10 kW input power. At least two coolers are needed for one generator unit, an additional one as backup is suggested.

For designing HTS generators with capacity of several MWs, a number of technical issues have to be considered, including HTS material properties, especially the dependence of  $I_c$  on the field and temperature; the electromagnetic design of the rotor and the stator; HTS coil winding techniques; rotor cooling techniques and low temperature rotary sealing; energy density in the stator and stator cooling; etc. As a conceptual demonstration of HTS generator design, a 10 MW HTS generator is proposed in the following paragraphs.

At the beginning of design, the key parameters of the generator are decided first. Here,  $P$ ,  $I$ ,  $V$  and  $n$  are designed according to the requirements of the wind farm and the power grid. As listed in Table 1,  $P$  is 10 MW from the design goal;  $V$  is 35 kV in 3 phases to meet the standard of substations; and phase current  $I$  is 165 A calculated from  $I = 0.577P/V$ . After that, the most important parameters to decide are the air gap field  $B_g$ , the generator output voltage  $V_g$ , current  $I_g$  and the number of phases in the stator.  $B_g$  is decided from the working conditions and the electromagnetic properties of the materials used. To obtain the size and weight advantages of HTS,  $B_g$  in HTS generator is often suggested as 1.0 - 1.4 T, much larger than that in the conventional ones.  $V_g$ ,  $I_g$  and the number of phases in the stator are depending on the materials, topology and structure of the stator, which are in much analogy to those in the "direct-driven" PM generators.

The rotor is designed with  $B_g$ ,  $n$ ,  $p$  and the gap width  $d$  as parameters. In HTS generator,  $d$  is usually much larger than that in conventional ones, because a cryostat must be inserted in

the gap to isolate the low temperature rotor from the room temperature parts. Considering the state of art Dewar technique,  $d$  of 10 - 20 mm can be suggested. The active length of the rotor  $l_g$  is decided according to the electromotive force  $E$  and the stator topologic design. Here,  $E$  can be estimated by  $E = Bglgv$ , where  $v$  is the linear speed of the rotor pole shoes,  $v = 2\pi nR_r$ . With  $p$  calculated from  $p = 60fg/n$ , and the properties of the HTS material used, the outer radius of the rotor  $R_r$  can be estimated using field design tools. Finally, referring to the stator material properties, the slot size and shape, as well as armature length and stator outer radius can be decided.

The key parameters of the conceptual model 10 MW "direct-driven" HTS generator are proposed and listed in Table 1. From a suggested scheme of coastal wind farm, the rotation speed  $n$  in this generator is 20 rpm and the rated generator output voltage  $V_g$  is 3000 V in 3 phases. Considering the converter capabilities and the control of the generator, the rated generator output frequency  $f_g$  is selected to be 10 Hz. Thus,  $p = 30$ . Applying the reported HTS coil design parameters (Li X. et al., 2010) to this model, the schematic view of the generator and the FEM estimated field distributions in the cross-section is shown in Figure 9. In this design, the excitation current of the rotor is 80 A, the FEM estimated air gap field at the inner radius of the stator  $B_g$  is about 0.98 T, and the maximum field in the HTS coil is about 0.55 T, as shown in the figure. Considering the properties of the HTS wires used here, the working temperature of the rotor is suggested to be 65 K.

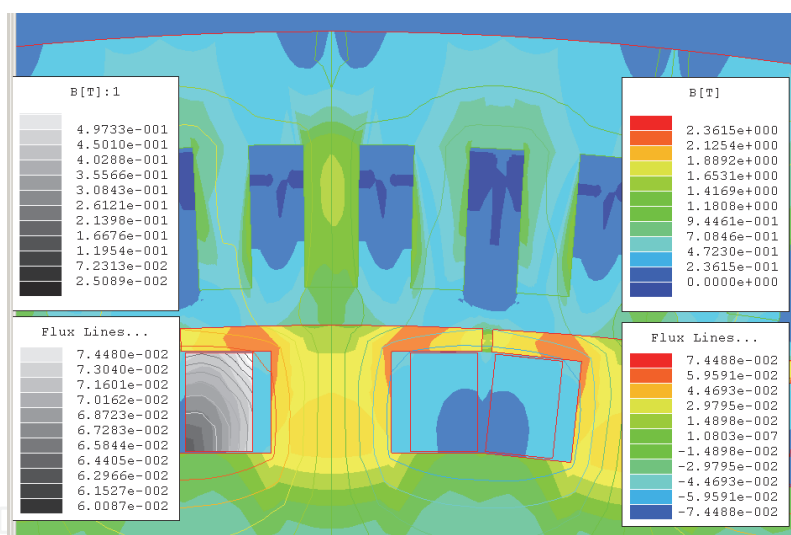


Fig. 9. The partial cross-section view with FEM results of the magnetic field distributions at 80 A working current in the 10 MW model.

The cross section dimensions of the excitation coils used here are taken from the reported 100 kW model. The coil is racetrack structured consists of 8 double pancakes. The scheme of the coil is shown in Figure 10 and the design parameters are listed in Table 1. Iron core can be used in the rotor to enhance the air gap field  $B_g$  and reduce the cost of HTS wire when the designed field of the generator is below 1.4 T. Epoxy plates are inserted between each of the pancakes and mounted at the both ends of the coils for enhanced insulation. To hold 60 such coils, the estimated circumradius of the rotor column is about 1528.6 mm. Taking the pole shoes into account, the rotor outer radius  $R_r$  is 1594 mm. With the 20 mm air gap, the inner radius of the stator is 1614 mm. Thus, the estimated electromotive force  $E$  is 1.65 V/m. At the suggested stator slot structure, where the stator outer radius is taken as 1750 mm,

thus the summed cross-section area of the stator windings is  $\sim 3831 \text{ cm}^2$ , and taking the electric current density in the stator windings as  $3 \text{ A/mm}^2$ , the active length of the stator armature is  $\sim 7.45 \text{ m}$ , and the estimated outline volume of this 10 MW model is  $3.5 \times 3.5 \times 7.7 \text{ m}^3$ , much longer than the reported European 10 MW HTS generator design (A. B. Abrahamsen et al., 2010). However, the European model is design to work at 20 K, where the current density in the excitation coil can be much larger than that at 65 K. On the other hand, because of the slim rotor and stator, the estimated weight of the 10 MW design here is only about 86 t, which may be advantageous in practical wind farm applications.

Rated output power (kW)	10000	Maximum field in rotor coil (T)	0.55
Rated system output voltage (kV)	35	Air gap width (mm)	20
Rated system output current (A)	165	Electromotive force (V/m)	1.65
Number of output phases	3	Rotor outer diameter (mm)	3188
Rated output frequency (Hz)	50	Active armature length (mm)	7450
Generator output voltage (V)	3000	Stator inner diameter (mm)	3228
Stator phase current (A)	1924.5	Stator slot area ( $\text{cm}^2$ )	3831
Number of stator phases	3	Stator outer diameter (mm)	3500
Rated generator frequency (Hz)	10	Stator Length (mm)	7550
Rated rotation speed (rpm)	20	Excitation coil width (mm)	156
Pairs of rotor poles	30	Excitation coil height (mm)	52
Rated excitation current (A)	80	Excitation coil length (mm)	7572
Rated air gap field (T)	0.98	Winding width (mm)	36
Rotor working temperature (K)	65	Pancake coils per pole	8
Rotor current density ( $\text{A/mm}^2$ )	8.5	Turns per pancake coil	40

Table 1. Key design parameters of the 10 MW HTS generator.

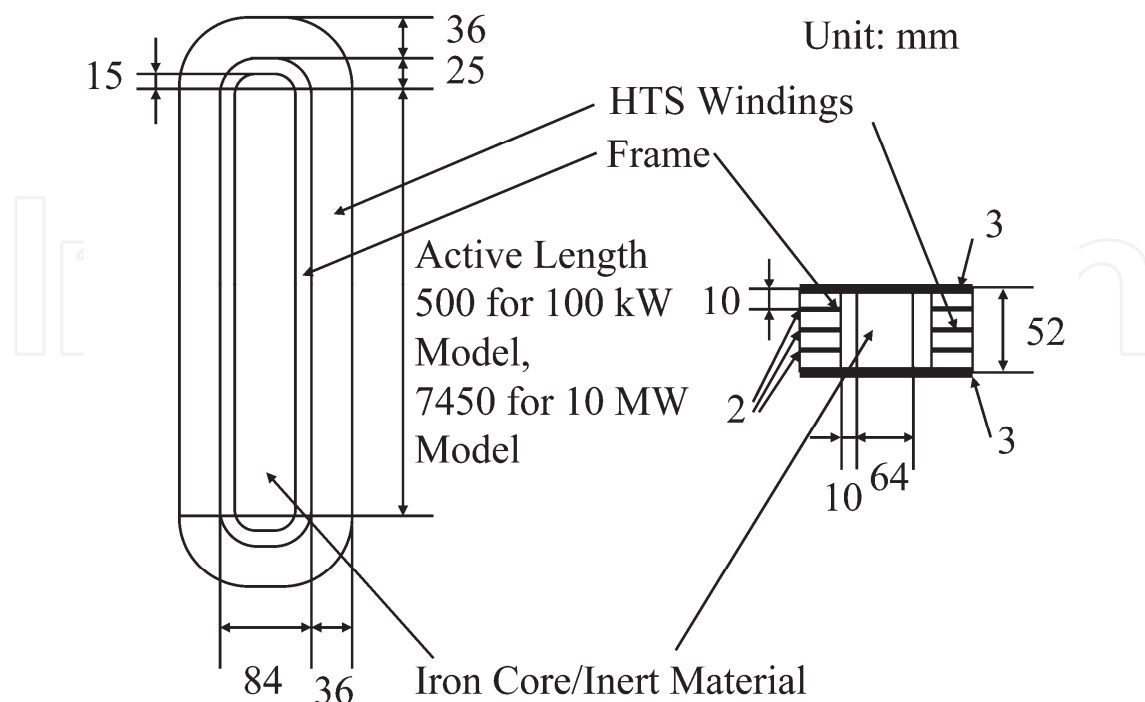


Fig. 10. Scheme of the excitation coil in the model generator.

### 3.2 Requirements of the HTS wire

HTS wire is the basis of the HTS generator and key to the performances. In practical using, the wire has to meet several basic requirements as listed below:

1. High critical parameters, especially  $j_c$  (B, T) which characterizes the ability of transmitting high current density at high magnetic fields and reasonable temperatures. Commercial HTS wires have  $j_c$  of more than  $10^4$  A/cm<sup>2</sup> at self field and 77 K, but the more important is  $j_c$  at pronounced field both parallel and perpendicular to the flat surface of the HTS wire. This is still very challenging for most wire manufacturers. Besides, the tolerance of the wire against over current shock and fluctuations are also important, as in a "direct-driven" wind turbine generator, when the driving force and/or the load varies, current pulses are directly applied to the excitation coils.
2. Long defect and splice free pieces with high mechanical strength and good uniformity. Even in laboratory usages, the demanded wire length is in term of kilometers. Although a few Ohmic contacts are usually allowed in coil winding, too many joints are harmful to the performance and operating safety, especially in the conduction cooling cases. Besides, for the design and winding convenience, the wire must be in good agreement with the nominal dimensions and  $j_c$ , and able to withstand the tensile and bending forces applied during coil winding, processing and operating.
3. Low AC losses. Although in synchronous generator the rotor is working at DC current and field, AC losses are still one of the important coil heating causes in magnetization and at fluctuations and current shocks. On the other hand, with low AC losses, HTS wires are able to be applied in the generator stator and other devices, such as cables and transformers.
4. Comparatively low costs. At present, commercialized Bi2223 wire costs about \$ 90/kAm, while its expected lowest market price is about \$ 50/kAm. Reports predicted that the YBCO wire will cost as cheap as \$ 10-15/kAm in the future, but no one can insurance when this price can be achieved in the market. The price is sometimes the main drawback to the practical applications of HTS devices, because although they are better in performance and more energy efficient, they are too expensive to be accepted by the industrial operators.

In this chapter, as a basic academic introduction to the HTS generator proposed to use in the wind farm, only the first issue is discussed based on several types of market available HTS wires. Table 2 listed the basic descriptions of them. Here, the "High strength" Bi2223, "344S" and "344C" YBCO tapes are manufactured by the American Superconductor Corp. (AMSC), the "SF4050" YBCO wire is manufactured by the SuperPower Inc., while the Bi2223 wire labeled as "Innost" is manufactured by Innova.

Figures 11 - 13 show the magnetic field and temperature dependences of  $j_c$  in some typical samples of HTS wires. Due to the strong anisotropy,  $j_c$  in HTS wire depends not only on magnetic field strength, but also on the direction of the applied field. At the same field,  $j_c$  is usually larger when the flat surface of the wire is parallel to the field than perpendicular to. Among different types of HTS wires, Bi2223 is usually much more field sensitive than YBCO, especially at comparatively high working temperatures. However, reports show in the high pressure processed Bi2223 wire,  $j_c$  (B, T) can be significantly enhanced. On the other hand, it is obvious that with the temperature decreasing, the critical current rises rapidly. At 60 K, for example, in most of the samples  $I_c$  at self field becomes about 2 times as large as that at 77K. Similiar enhancement of  $j_c$  by lowering the temperature is also observed

at pronounced fields. Therefore, instead of 77 K, the working temperature is often selected as 20 – 65 K in the devices requiring high fields, as suggested here in the 10 MW model.

Type of HTS wire	344C	High Strength	344S	SF4050	Innost
Superconductor	YBCO	Bi2223	YBCO	YBCO	Bi2223
Stabilizer/matrix	Cu	Ag	S. S.	None	Ag
Thickness (mm)	0.18 - 0.22	0.255 - 0.285	0.275-0.31	0.055	0.19 - 0.25
Width (mm)	4.27 - 4.55	4.2 - 4.4	4.27-4.55	4.0	4.0 - 4.4
Bend diameter* (mm)	25	38	25	25	70
Tensile stress* (MPa)	200	200	300	550	80
Tension* (N)	120	210	200	-	110
Tensile strain @ 77K*	0.3%	0.4%	0.3%	0.45%	0.2%
$I_{c0}$ @ self field, 77 K (A)	90	145	90	80	110

\*Greater than 95%  $I_c$  Retention.

Table 2. Parameters and properties of the HTS wires proposed to use in the rotor.

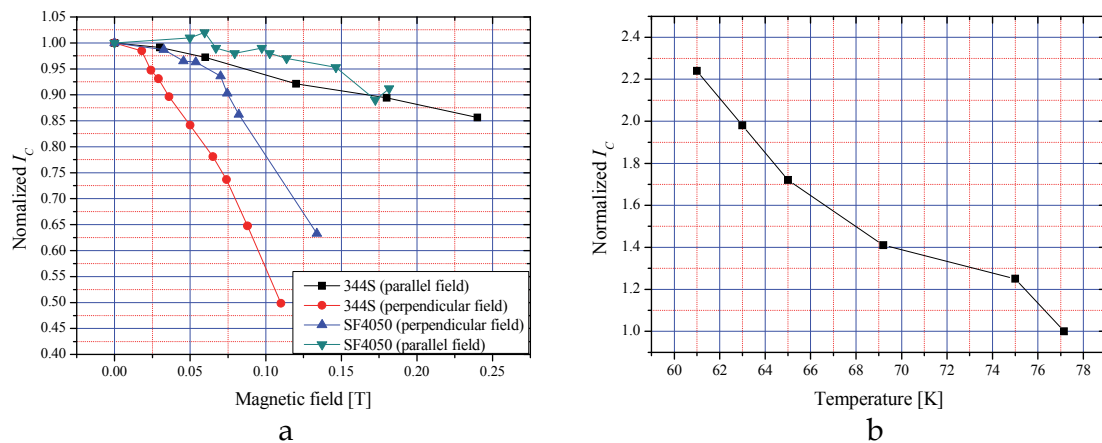


Fig. 11. Normalized  $I_c$  vs. field (a) and temperature (b) in wires from SuperPower and AMSC.

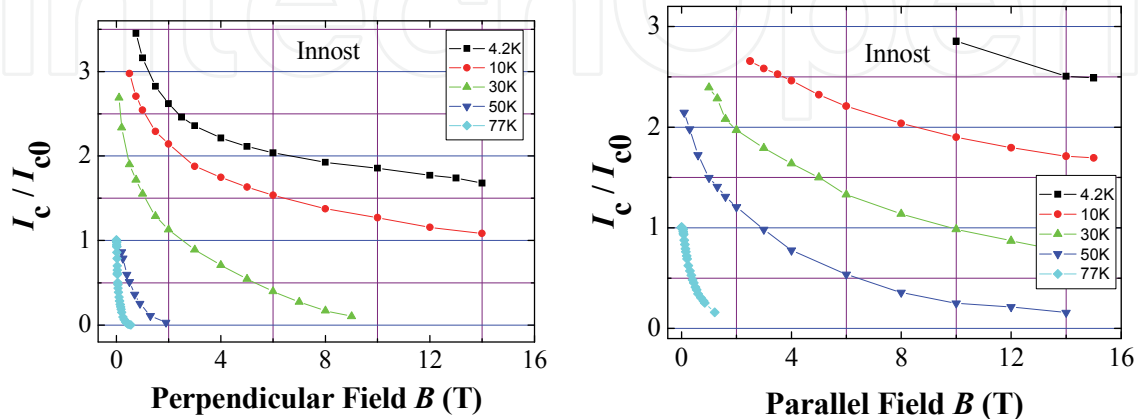


Fig. 12. Normalized  $I_c$  vs. field and temperature in wires from Innova.

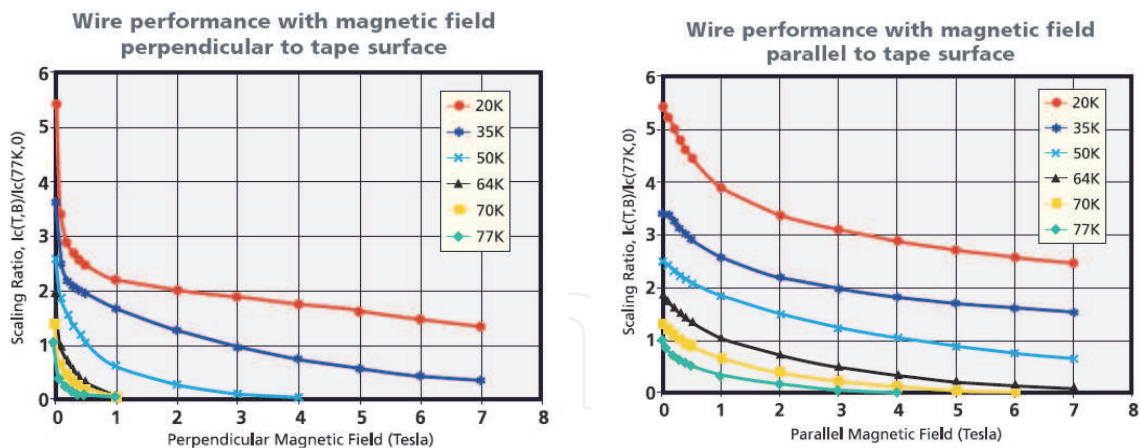


Fig. 13. Normalized  $I_c$  vs. field and temperature in Bi2223 wires from AMSC (AMSC 2009).

Besides the critical current vs. field and temperature relationships, the thermal stability and properties against pulsed current shocks in the HTS wires are also important in the design of HTS devices. It is difficult to predict the responses of HTS wire at variable over-current pulses just from theoretical models. Hence, U-I curves in wire samples are measured using 4-electrode method at liquid nitrogen immersion and quasi-adiabatic conditions simulating the heat transfer environments in the coil. The thermal insulation of the latter is made by wrapping several layers of fiberglass cloth around the about 20 cm long sample, and then solidified it in epoxy. Typical pulsed current shock waveforms are shown in Figure 14.

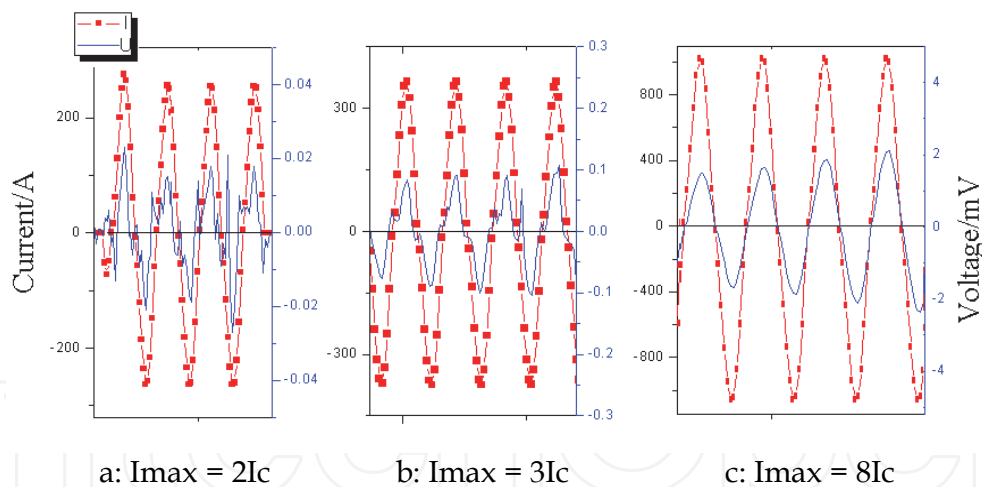


Fig. 14. Waveforms of the U-I responses in Bi2223 tape at pulsed currents of  $I_{max} = 2I_c$ ,  $3I_c$  and  $8I_c$ , with duration  $t = 200$  ms, in quasi-adiabatic environment.

From Figure 14, U-I results with the peak value of the pulsed 50 Hz AC current  $I_{max}$  up to  $8I_c$  and the duration  $t = 200$  ms show that during the over-current pulse, the voltage across the sample, essentially the sample resistance increases with time, indicative of a typical heat up response. Afterwards, in the setup of the experiment here, continuous working current  $I_w$  is applied to the sample to monitor the recovery processes. Figure 15 shows typical recovery results in Bi2223 and YBCO wires with different cooling conditions. Careful tests show that the possibility and time of recovery depend directly on the energy injected by the pulse and the continuous working current  $I_w$ . Three types of recovery can be identified. The first is

immediate recovery, with only slight temperature and resistance rising. As shown in Figure 14a, the U-I responses in this case show obvious reentry into the superconducting state within the period of the applied AC pulses. This indicates the heat is not accumulating in the sample. The second is delayed recovery, the reentry within the period is not obvious as shown in Figure 14b, and the recovery time can be ranged from several ms to 10 s, with the maximum sample temperature up to 200 K. Nevertheless, in this case the sample is able to reenter the superconducting state without turning off the working current. Figure 15 shows typical recovery results in this case. Here the resistance in the coil increases obviously and quickly at the occurring of the over-current, which makes it a “fault current limiter” against the pulsed current and protect itself from continuous heating up. This can be an additional advantage for the application of HTS generators in wind farms because the wind and load are frequently fluctuating. The third, however, is irrecoverable. As shown in Figure 14c, at large over-current shock and/or long pulse duration, the sample is quick and continuously heat up, indicated by quick and continuously rising of the voltage across the sample. In this case, if the working current in the coil cannot be cut off within several seconds, the coil would be directly burnt by the accumulated heat. Hence, sensors and circuit breakers are necessary in the HTS generator to demagnetization the rotor at large current shocks.

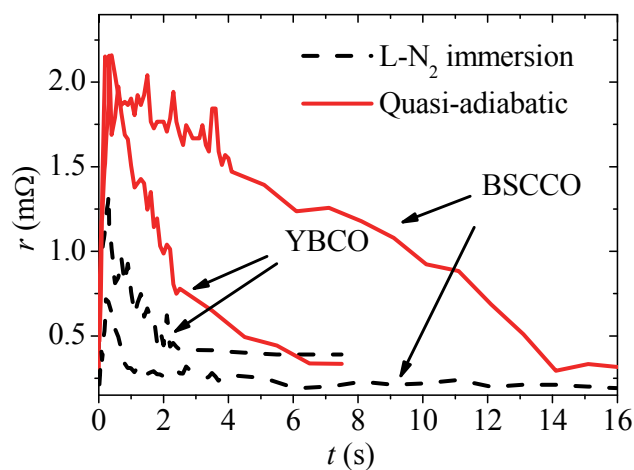


Fig. 15. Pulsed current shock recovery characterized by resistance – time correlation curves obtained at different cooling conditions in Bi2223 and YBCO wires.

### 3.3 Rotor coil winding and testing

To check the feasibility of the proposed 10 MW model, especially the rotor coil design and winding techniques, a 100 kW model generator with 6 poles and active length of 500 mm is developed first. The dimension parameters of the coil in the 100 kW generator are listed in Table 3. Unlike in conventional racetrack coils, the corner radius here is limited by the rated minimum bending radius of the HTS wire to keep the  $I_c$  properties. Besides, as the market available HTS wires are all in flat tape shape and can withstand little twisting stresses, the excitation coil on the pole is in stacked double pancake structure instead of the solenoid one. The otherwise design techniques are in much analogy to those in conventional synchronous generators. With designed working current of 50 A, FEM field simulation shows a gap field of  $\sim 0.91$  T at the inner radius of the stator, and the maximum field at the coil, with DT-4 iron core to control the field distributions, is  $\sim 0.3$  T. Thus, wires with  $I_c(B) > 50$  A at 0.3 T field is required. FEM results of the field distributions in the coil show that the high fields

occur at the upper part and the lower-inner corner in the cross section of the coil, with a significant part of the field perpendicular to the flat wire surface. Hence, it is challenging to run this model at 77 K, because few wires have  $I_c > 50$  A at 0.3 T perpendicular field. It is possible to enhance the current carrying capacity of the wire by lowering the temperature, and consequently enhance the energy density.

Frame corner radius	Frame width	Frame length	Coil height	Wire used (m)
25	84	550	52	2569
Outer corner radius	Coil width	Coil length	Winding height	Turns per coil
61	156	622	10	320

Unit: mm (if not labeled)

Table 3. Parameters of the HTS coil proposed to use in the rotor of 100 kW model.

A test racetrack coil is fabricated according to the parameters listed in Table 3. For electrical insulation, the wire is wrapped by 3 layers of Kapton film before winding. The thickness of each layer is about 0.01 mm. Thus, the thickness and width of the wire with insulation are about 0.42 - 0.46 mm and 4.26 - 4.51 mm, respectively. In coil winding, the middle point of the wire is firstly mounted to the inner frame and the wire is then wound towards both ends. To improve the thermal conductivity and mechanical strength, the coils are impregnated in a mixture of low temperature epoxy DW-3 and AlN powders with the weight ratio of epoxy : AlN = 3 : 1. After winding, the coil is heated to 60 °C while continuously rotating for about 1 hour to solidify the epoxy. Due to insulation, epoxy addition and other effects in winding, the mean thickness of the turns expands to about 0.9 mm, while the mean thickness of the double pancake coil, which consists of twice of the wire width, is about 10 mm including a 0.5 mm thick epoxy resin insulation plate. After winding and solidifying, the E-I characteristics and the field distributions of the test coil are measured in liquid nitrogen immersion, and the E-I curves are shown in Figure 16.

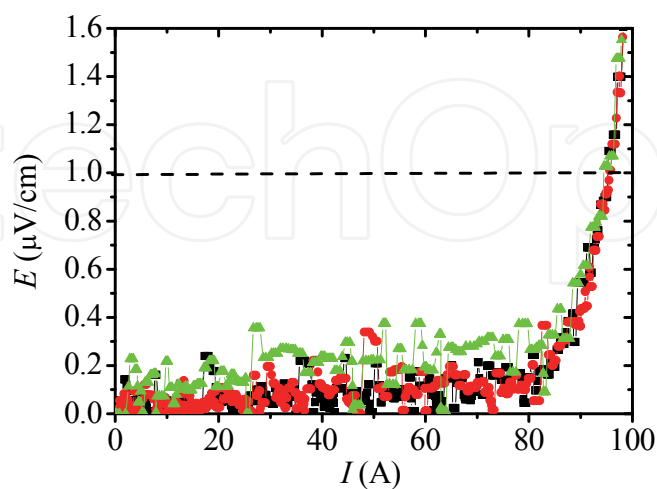


Fig. 16. E-I results in the test coil at three times repeated magnetization up to 100 A.

According to the  $1\mu\text{V}/\text{cm}$  criteria,  $I_c$  of the coil is  $\sim 96$  A, much smaller than that of the original wire, which is  $\sim 145$  A. This degradation can be attributed to the perpendicular field

generated by the coil. Field distributions obtained by precise Hall sensor show that at 80 A working current, the field at the coil center is  $\sim 0.12$  T and the maximum perpendicular field at the outer side is  $\sim 0.17$  T. Three times of repeated magnetization up to 100 A with current saturating at 100 A for about 10 minutes cause no further  $I_c$  degradation and demonstrate the overload stability of the test coil.

From the above, the design concept of HTS wind turbine generator is proposed and some of the most important issues are discussed with a primary test result in a 1:1 sized test coil using commercial Bi2223 wire. The results shine a few lights on the future applications of the HTS generator in the wind farms. However, there are still a lot of works to do.

#### 4. SMES in wind farms

SMES is an energy storage device can achieve high power density with quick response and little energy losses. Utilizing superconducting materials, the current density in SMES is 1 - 2 orders of magnitudes higher than that in the conventional energy storage coils. Due to the extremely low DC resistance, the energy stored in SMES can be kept for a period of longer than several days without significant losses. Besides, because SMES is free of energy form transition during the process of energy exchanging, it is advantageous in energy conversion efficiency, too. The energy losses in SMES are mainly rectifier/inverter losses and the power consumed by refrigeration. For HTS wire based SMES, the energy storage efficiency can be up to 94%.

With the advantages described above, SMES is able to adjust the active and reactive power in the grid, as well as compensate the voltage and current surges, especially in renewable power plants. For example, in wind power plant, the fluctuation caused by the wind can be smoothed by SMES installed between the wind turbine and the grid, and the output voltage and frequency are then regulated to meet the requirements of the power grid. Besides, SMES can also provide backup power for the coolers, the control system and the excitation power supply in the wind farm.

##### 4.1 Structure and functions of SMES

Figure 17 shows a typical diagram of SMES connected to the power grid. It usually consists of a HTS coil to store the electromagnetic energy, which is installed in a cryostat and cooled by a cryocooler system; a reversible AC/DC converter acts as the rectifier/inverter to charge and discharge the coil; a pair of current leads connect the coil and the converter; a controller gathers the diversity signal from the power grid and the monitor signal from the magnet to generate the activation pulses and drive the converter. Commonly, the activation pulses are PWM type, which can modulate the converter output to desired waveforms. At fluctuations, a compensate signal is generated from comparing the ideal waveform to the practical ones in the grid. With this signal and the energy stored in HTS coil, SMES can work as a dynamic voltage regulator (DVR) as well as an emergency backup power supply. These functions are useful in renewable power plants which often encounter fluctuations from the resources and loads, and can help them to meet the voltage and frequency stability requirements from the main frame of the grid.

A suggested operation model in wind power plant with SMES is shown Figure 18. Currently, wind turbine will be directly cut off while encountering over-speed of wind for the safety of the instruments. However, this is harmful to the power grid stability because as shown in Figure 18 in solid line, with such working mode, the power generated from the

wind plant will drop suddenly to zero at point b shortly after it reaches the maximum. In a friendlier operation mode, the grid demands a little “inert” in the output power, aka a turn-off period within several seconds similar to that in thermal and hydro plants. With SMES, this demand is easy to fulfill. Utilizing the energy stored in the coil and the ability of waveform tailoring by the converter, SMES can give enough additional active power to simulate the “inertial” turn-off output, as illustrated in section c of Figure 18 by dashed lines. With this ability, the compatibility between the wind farm and the grid can be significantly improved. It is very helpful to overcome the technical barriers limiting the capacity of wind power connected to the grid.

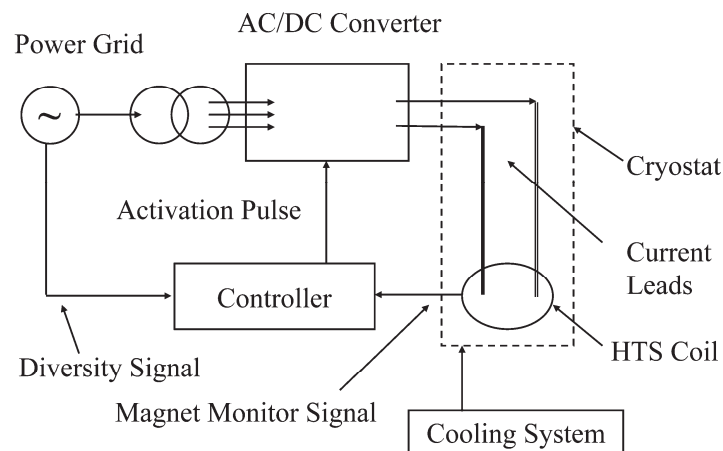


Fig. 17. Schematic diagram of SMES.

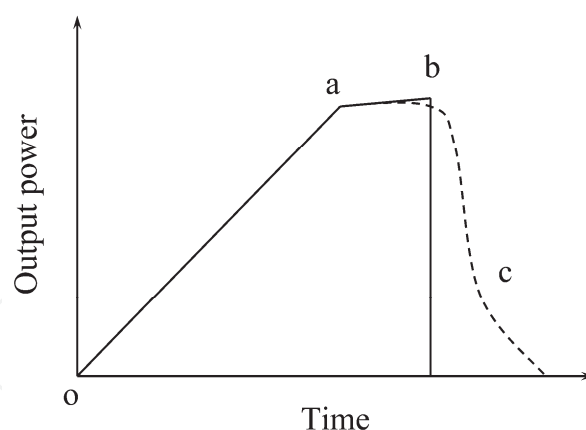


Fig. 18. Suggested operation model of SMES in the wind farm at over-speed of wind. Point a, rated output at rated speed; b, turbine is cut off at over-speed, output would jump to 0 (solid line); c, with SMES, several seconds of “inertial” output available (dashed line).

#### 4.2 Design concept of SMES using HTS wire

The first concern in SMES design is the scale and application purposes. There are roughly three levels of scales for SMES. The small has capacity of  $\sim 0.1\text{MWh}$  that can supply several minutes of output at the end user voltage and  $\sim 1000\text{ A}$ . It is suitable for small power plants as photovoltaic stations, stand alone wind turbines, and emergency generators; functioning

as a stabilizer against the fluctuations; as well as supplying active and reactive powers for power factor correcting, phase balancing and temporary supporting to the very important loads. The medium has capacity of  $\sim 10$ MWh and can supply several minutes of output at distribution substation level. It can be installed in distributed power generating stations (DG) and middle-sized power plants to smooth fluctuations, regulate frequency and voltage, and improve the output stability and quality. Large SMES with capacity of  $\sim 1$ GWh or more can supply the output energy for several hours or even longer at the level of main-frame power transmission grids. Such SMES can work as hot backup and DVR for power system, as well as peak load adjusters and switch-connectors in the grid. In wind farms, small and medium scaled SMES are usually enough for improving the conditions of connecting to the grids.

Table 4 lists a proposed HTS magnet design for a 10 MJ - 10 MW SMES designed as output regulator for the substation level, for example, at the output end of 10 MW wind turbine. As shown in the table, the maximum field in the solenoid coil is 8.94 T. According to the  $j_c$  (B, T) results shown in Figure 12, the working temperature of this SMES is selected as 10 K. Although this temperature is relatively low and the consumption of cooling power is much higher than that at 77 K, the SMES is still advantageous in energy efficiency comparing to that with low temperature superconducting wires, which must work at 4.2 K.

Type of coils	Inductance	Maximum field	Coil height	Peak power
4-solenoid	4 x 8.9 H	8.94 T	700 mm	10 MW
Rated voltage	Energy stored	Coil inner radius	Coil outer radius	Turns per coil
10 kV	10 MJ	157 mm	270 mm	$\sim 77000$

Table 4. Design parameters of 10 MJ - 10 MW model SMES using HTS wires.

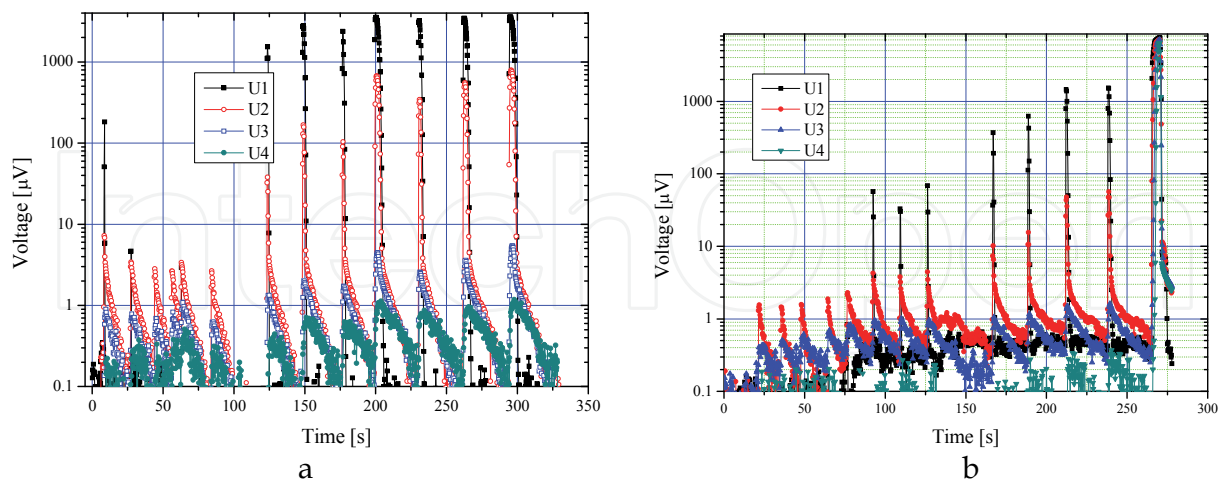


Fig. 19. Thermal heating induced quench in HTS wires working at 0.5 (a) and 0.9 (b)  $I_c$ .

Besides the  $j_c$  (B, T) concerning, the properties at quick charging and discharging are also very important. In the model described above, when the peak power is 10 MW, the output current in the coil is  $\sim 416$  A, which is about 2 - 3 times as large as the  $I_c$  at 10 K and  $\sim 9$  T field in the proposed HTS wire. Parallel connection is used here to allow more wires share

the peak current. However, in full discharge process, the wire is at temporary over-current, while quench initiation and propagation may occur because of temporary heating. Figure 19 shows experimental results in HTS wires at thermal heating induced quench propagation at working currents of  $0.5 I_c$  and  $0.9 I_c$ , respectively.

In the experiment, four traces are recorded to monitor the voltages across a series of voltage contacts in the HTS wire. At working current of  $0.5 I_c$ , the heating current is  $0.5 - 0.62A$  with  $0.01A$  increments, and the duration of the heating pulse is  $300ms$ , while at  $0.9 I_c$ , the heating current is  $0.28 - 0.42A$  with the same increments and the duration. Each set of peaks in the figure stands for a pulsed thermal shock. According to the results, at  $0.5 I_c$ , irrecoverable quench occurs at the heating current of  $0.62A$ , while at  $0.9 I_c$ , the same phenomenon shows when the heating current is  $0.42A$ . On the other hand, quench propagation starts at  $0.34A$  heating current for  $0.5 I_c$  working current, corresponding to the quench initiation energy of  $0.52 J$ , while in  $0.9 I_c$  cases, quench propagation starts at  $0.25 A$  heating current, corresponds to the quench initiation energy of  $0.28 J$ . Besides, dividing the distance between contacts by the delay time of quench in corresponding sections, the quench propagation speed NZPV in sample can be calculated. The minimum quench energy (MQE) can also be estimated from extracting the quench initiation energy injected into the wire. In Figures 20a and 20b the NZPV and MQE in typical HTS samples are shown. As demonstrated in the figures, NZPV depends sensitively on the working currents, which indicates succeeding heating in seconds after the over-current shock may accumulate in the wire and start quench. Therefore the effects of different working currents must be considered in MQE estimation, and in SEMS design, working current should be carefully selected to avoid succeeding heat accumulation.

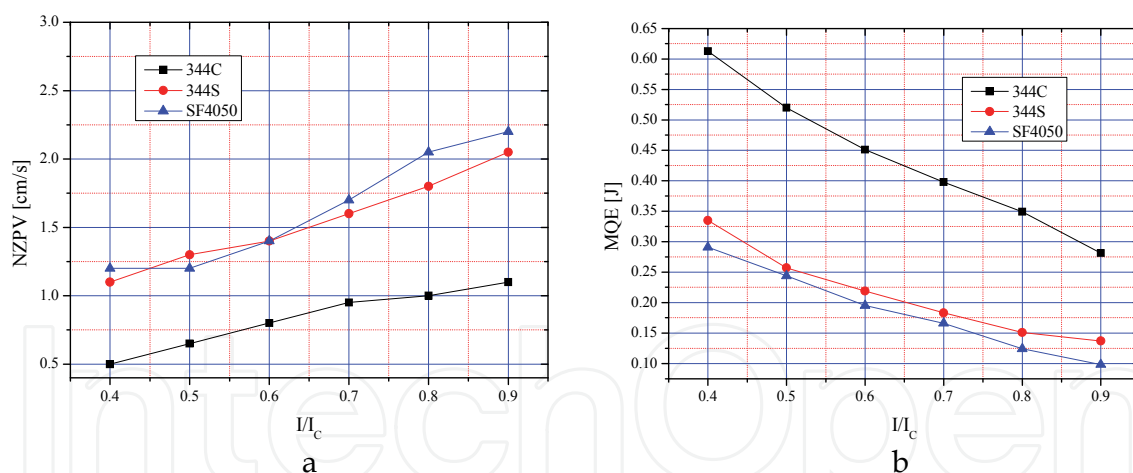


Fig. 20. NZPV and MQE in typical HTS wire samples estimated from voltage-time records of thermal heating induced quench propagation.

In total, development of SMES using HTS is still in the very primary stage. Attempt to build and operate an  $1 MJ/0.5 MW$  HTS SMES was done in China in 2006 – 2008, the system is in substation level with rated voltage of  $10.5 kV$  aiming to be DVR and active filter against the fluctuations in the sub-grid caused by the inductance loads such as motors and fluorescent lamps. The test operation of the HTS coil was successful with full charge/discharge current of  $\sim 600 A$ , but the waveform regulator was not as stable as expected. This result shows not only the HTS techniques need further exploration for MW level SMES applications, but also the power electronics require in depth research and many more test operations.

## 5. SFCL in wind farms

Fault current limiter is a novel device developed quickly in the recent decade. In principle, it is a device with variable resistances which can show small resistance at the rated current and show large effective resistance at over-currents. From the state transition curve shown in Figure 1, superconductor is excellent candidate to fault current limiter. Superconducting fault current limiter (SFCL) was proposed shortly after the commercial HTS wire is available. However, in practical operation, it is not so simple to achieve even substation level SFCL as that expected. The key problem in SFCL is finding suitable method to transform microscopic effects to macroscopic ones with high energy efficiency, quick response and recovery, and safety as well. In wind farms, SFCL can be utilized as over-current protection for generators and bus buffer against surges from the grid and/or adjacent wind plants. In such usage the over-current is  $\sim 1000$  A, with voltage around 35 kV. This makes a market for MW level SFCL.

Various topologies and structures are proposed for SFCL in the past years. Currently, SFCL of the bridge type, the resistance type and the magnetic saturation type are tested in grids and promising in industry applications. Figure 21 shows schematic structures of these types.

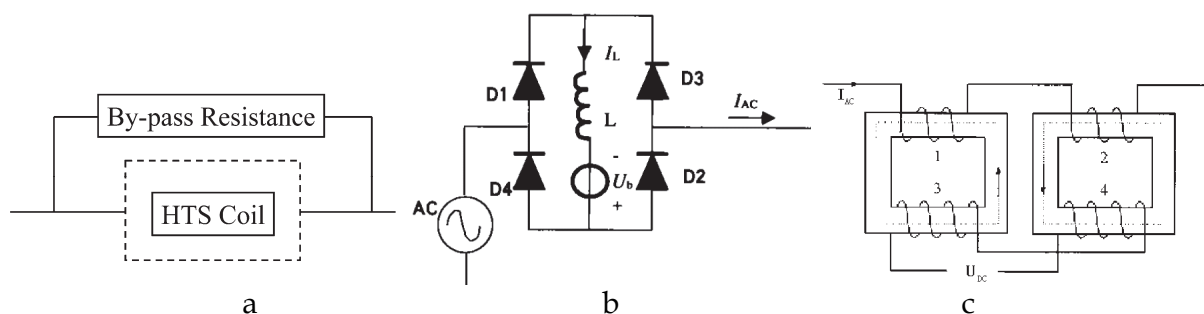


Fig. 21. Schematic structures of SFCL in the resistance type (a), bridge type (b) and magnetic saturation type (c).

Many prototype SFCL use the superconducting state transition to generate an appropriate resistance and achieve its current limiting functions. According to the definition of  $j_c$ , when the fault disappears, SFCL can automatically reset and the circuit protected by the SFCL will then return to its low resistance state. As shown in Figure 21a, the resistance type SFCL uses directly the normal state resistance to limit the fault current. It is simple and combines the fault detection and reaction together, thus quick in response at most cases. The drawbacks of the resistance type SFCL are the comparatively long recovery time depends on the cooling conditions and pronounced heat generation at the current limiting stage. The bridge type in Figure 21b combines the effects of DC resistance and the inductance of the HTS coil. At the rated current, the AC part of the current applied to the coil is overridden by DC bias, and no obvious voltage dropping occurs across the coil. However, at faults, when the peak value of the current rises to larger than the bias, the AC parts will take effects in the coil and generate both resistance and impedance, which in turn limits the current. The bridge type SFCL is also quick in response with short recovery time, but the structure is complex and its capacity depends on the diodes forming the bridge. The magnetic saturation type shown in Figure 21c utilizes both high current density in HTS wires and nonlinear magnetic responses in the iron core. In this type of SFCL, when the current is small, the field generated by the DC bias in the HTS coil is captured in the iron core and saturates it deeply, thus the AC winding

presents low impedance, while at faults, the high field caused by the large current drives the iron core into and out of saturation, and the impedance of the AC windings will increase rapidly to limit the fault current.

In principle the requirement of HTS wire in SFCL is similar to that in SMES, especially the over-current tolerance and quench properties are emphasized. In the resistance type SFCL, however, the resistance after superconducting to normal-state transition needs to be as large as possible. Special HTS wire structure is developed for resistance type SFCL, characterized by ultra thin stabilizing layers or stabilizing layers/matrix with high resistivity. Besides, as AC currents and/or currents with AC parts are often applied to SFCL, the AC losses in HTS wire need to be carefully considered. Figure 22 shows the AC losses measurement results in typical HTS wires. From the results, it is demonstrated that in Bi2223 wires, the AC losses can be predicted by the Norris model, while in the YBCO wire with magnetic substrate of Ni : W alloy, extra AC losses caused by the substrate magnetization must be added to the total losses. Similar effect is also observed in MgB<sub>2</sub>/Fe wires (X. Du, 2010). This is somehow disadvantageous in SFCL usages.

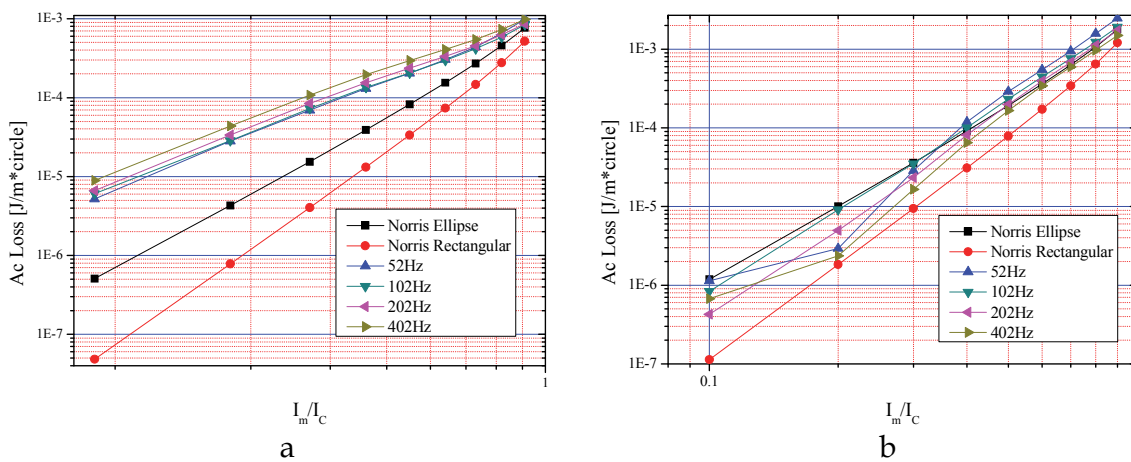


Fig. 22. AC losses in 344C YBCO (a) and Bi2223 (b) superconducting wires compared with the predictions of the Norris model.

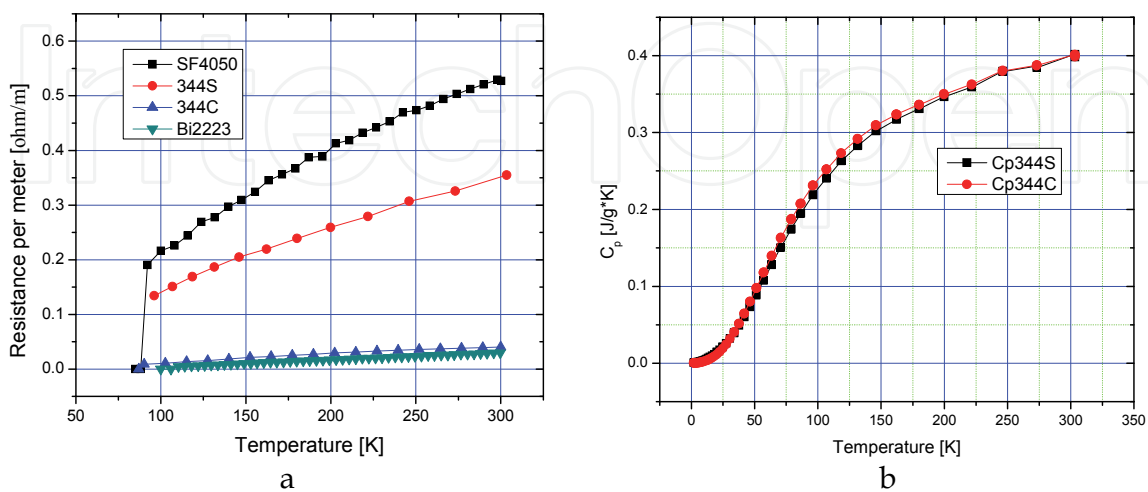


Fig. 23. Resistance (a) and heat capacity (b) as functions of temperature measured in HTS wires.

Besides, as HTS wires in SFCL are often working in the normal state, and the temperature in the SFCL can be as high as  $\sim 200$  K after fault current shocking, the normal state resistance and heat capacity in the wires as functions of temperature are to be investigated, especially for the resistance type SFCL. Figures 23a and 23b show the experimental results of normal state resistance and heat capacity in typical HTS wires. By cooperation with manufacturers, it is possible to tailor the properties of the wire, and design SFCL with the best current and thermal responses.

A prototype resistance type SFCL is designed and tested aiming to over-current protection in HTS wind generator. In this case, the fault current is commonly below 1000 A, with pulse duration of several seconds. A matrix structure with 4 coils is designed, each two of them are serial connected, and the two branches are parallel connected. The photo of the SFCL is shown in Figure 24. In test operations of this prototype, with  $0.1 \Omega$  line resistance and  $1.4 \Omega$  by-pass resistance, the peak fault current is suppressed from 4524 A to 1017 A at 320 V short circuit voltage, while the steady state current is  $\sim 600$  A after the 4th cycle (80 ms). At 360 V, the peak suppression is from 5090 A to 1050 A, and the saturated current is 620 A. This pilot experiment demonstrates the ability of protecting the magnetization and power generation coils in HTS generator and similar devices using simple structured SFCL.



Fig. 24. Prototype SFCL and test circuitries.

## 6. Other HTS devices

Besides the devices above, there are many more possibilities utilizing the superconducting techniques, such as HTS cables and transformers. Superconducting power transmission cable is a high current density device with very low resistance that works both at AC and DC currents. In wind farm, HTS cables can be the connector between the generator and the converter, and/or between the converter and the bus. In principle, superconducting cables are suitable in high current density and short distance transmission. As the energy loss in HTS cable, even counting on the AC losses, is much lower than that in conventional metal cables, HTS cable is significantly power saving. Moreover, HTS cable can also act as SFCL at over-currents, if the resistance and current capacity are carefully selected. HTS transformer

is also advantageous in the energy density with lower losses at the high current part. The combination of HTS transformer, HTS cable, SMES and HTS generator will show additional advantages by sharing the cooling system and simplifying the current leads since the low temperature parts can be connected together, with only one room temperature outlet at the end that connecting to the grid, as shown in Figure 25. The technical barriers of widely applying HTS devices in wind farm are the comparatively high prices, complex installation and operation with the low temperature systems, and lack of opportunities to operate with large electrical devices and the power grid.

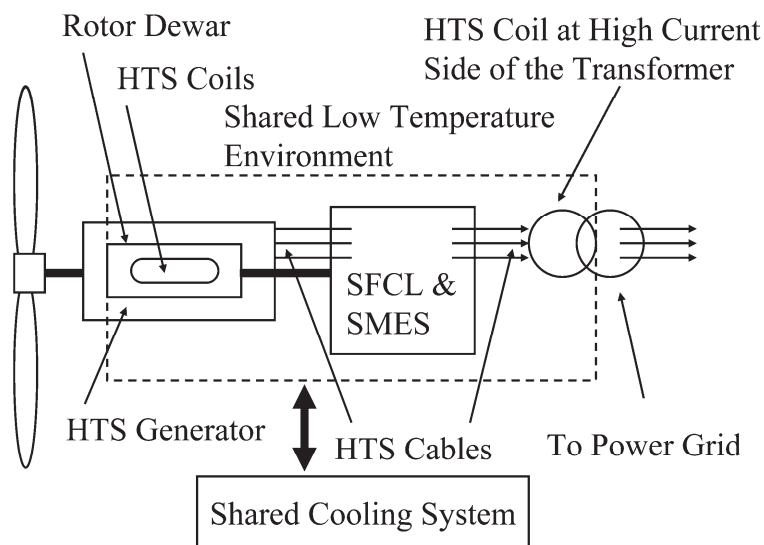


Fig. 25. Combination of HTS devices in the wind farm.

## 7. Conclusion

After the developing of superconducting techniques during the past century, more and more devices are invented and developed, and several of them are suitable to be applied in electrical power applications, especially in the renewable power plants such as wind farms. It is expectable that in the near future, HTS generators in 10 MW capacity, as well as SMES, SFCL, HTS cable and transformer are able to be utilized in the novel wind farm, and further enhance the economic profits as well as the serving abilities to the power grid. From now on, efforts concerning test operations at practical conditions of HTS power devices in both wind farms and substations are to be emphasized.

## 8. Acknowledgment

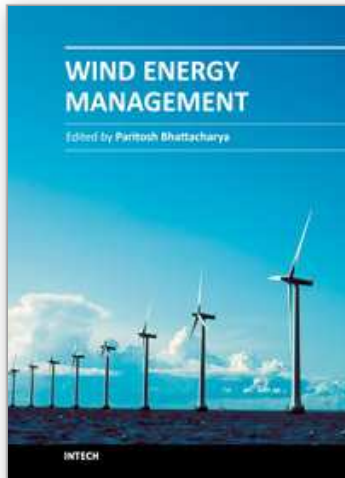
The author thanks heartily to Dr. Yigang Zhou and Dr. Xiaoji Du from Institute of Electrical Engineering, Chinese Academy of Sciences for supplying designing ideas and testing data. Thanks to Editor Ms. Romina for kindly contacts. This chapter is partially supported by the high-tech program from MOST of China, Grant No. 2008AA03Z203, and the NSFC project, Grant No. 50507019.

Special thanks to my beloved May.

## 9. References

- H. Kamerlingh Onnes. (1911). Commun. Phys. Lab. Univ. Leiden. Suppl. 29
- W. T. Norris. (1969). Calculation of hysteresis losses in hard superconductors carrying ac: isolated conductors and edges of thin sheets, *J. Phys. D: Appl. Phys.* 1930, Vol. 3, pp. 489-507
- W. J. Carr, Jr. (1983). AC loss and macroscopic theory of superconductors, Gordon and Breach, Science Publishers, Inc., ISBN 0-677-05700-8, New York, USA
- Li, X., Zhou, Y., Han, L., Zhang, G., et. al. (2010). Design of a High Temperature Superconducting Generator for Wind Power Applications, *IEEE Trans. on Appl. Supercond.* To be published in ASC 2010 suppl. issue, ISSN: 1051-8223
- A. B. Abrahamsen, N. Mijatovic, E. Seiler, T. Zirngibl, C. Træholt, P. B. Nørgard, N. F. Pedersen, N. H. Andersen and J Østergard. (2010). Superconducting wind turbine generators, *Supercond. Sci. Technol.* Vol. 23, 034019
- American Superconductor Corp. Data Sheet and Press Release, Feb. 10<sup>th</sup>, 2009
- Xiaoji Du, Doctoral thesis, 2010

IntechOpen



## **Wind Energy Management**

Edited by Dr Paritosh Bhattacharya

ISBN 978-953-307-336-1

Hard cover, 128 pages

**Publisher** InTech

**Published online** 22, September, 2011

**Published in print edition** September, 2011

The book "Wind Energy Management" is a required part of pursuing research work in the field of Renewable Energy at most universities. It provides in-depth knowledge to the subject for the beginners and stimulates further interest in the topic. The salient features of this book include: - Strong coverage of key topics - User friendly and accessible presentation to make learning interesting as much as possible - Its approach is explanatory and language is lucid and communicable - Recent research papers are incorporated

### **How to reference**

In order to correctly reference this scholarly work, feel free to copy and paste the following:

Xiaohang Li (2011). Superconducting Devices in Wind Farm, Wind Energy Management, Dr Paritosh Bhattacharya (Ed.), ISBN: 978-953-307-336-1, InTech, Available from: <http://www.intechopen.com/books/wind-energy-management/superconducting-devices-in-wind-farm>

**INTECH**  
open science | open minds

### **InTech Europe**

University Campus STeP Ri  
Slavka Krautzeka 83/A  
51000 Rijeka, Croatia  
Phone: +385 (51) 770 447  
Fax: +385 (51) 686 166  
[www.intechopen.com](http://www.intechopen.com)

### **InTech China**

Unit 405, Office Block, Hotel Equatorial Shanghai  
No.65, Yan An Road (West), Shanghai, 200040, China  
中国上海市延安西路65号上海国际贵都大饭店办公楼405单元  
Phone: +86-21-62489820  
Fax: +86-21-62489821

© 2011 The Author(s). Licensee IntechOpen. This chapter is distributed under the terms of the [Creative Commons Attribution-NonCommercial-ShareAlike-3.0 License](#), which permits use, distribution and reproduction for non-commercial purposes, provided the original is properly cited and derivative works building on this content are distributed under the same license.

IntechOpen

IntechOpen